# Vertical Profiles of $^{226}$Ra and $^{228}$Ra Activity Concentrations in the Western Subarctic Gyre of the Pacific Ocean

Hirofumi Tazoe[1]*, Hajime Obata[2], Takuya Hara[2], Mutsuo Inoue[3], Takahiro Tanaka[4] and Jun Nishioka[5]

[1] Institute of Radiation Emergency Medicine, Hirosaki University, Hirosaki, Japan, [2] Atmosphere and Ocean Research Institute, The University of Tokyo, Kashiwa, Japan, [3] Low Level Radioactivity Laboratory, Institute of Nature and Environmental Technology, Kanazawa University, Nomi, Japan, [4] Fisheries Resources Institute, Japan Fisheries Research and Education Agency, Shiogama, Japan, [5] Institute of Low Temperature Science, Hokkaido University, Sapporo, Japan

The vertical activity concentration distributions of the radium isotopes, $^{226}$Ra and $^{228}$Ra, which are useful as radiotracers, were obtained for the first time in the western Subarctic Pacific Gyre (WSAG). It was possible to detect short-lived $^{228}$Ra present from the surface to 400 m depth by analyzing large seawater samples. Low $^{228}$Ra and high $^{226}$Ra activity concentrations in the surface layer in the WSAG were strongly influenced by upwelled deeper water with nutrients. The activity concentration distribution of $^{226}$Ra especially was in good agreement with the silicate concentration distribution, which was consistent with previous reported findings. These distributions were uniform from the surface to 100 m of the dichothermal layer due to vertical mixing in winter. $^{228}$Ra activity concentration decreased with water depth below the pycnocline and reached the undetectable level at 600 m which was within the oxygen minimum layer. Estimations of vertical fluxes of $^{228}$Ra and nitrate according to $^{228}$Ra decay indicated that the vertical transport by eddy diffusion was a minor process for the $^{228}$Ra and nitrate fluxes, and lateral transport mainly affected $^{228}$Ra in the intermediate warm water, that is, the mesothermal layer below the main pycnocline. Vertical mixing or submarine underground water and lateral transport to the WSAG could yield this $^{228}$Ra in the intermediate depth.

Keywords: radium-228, radium-226, Subarctic Gyre of the Pacific Ocean, vertical flux, lateral transport

## INTRODUCTION

Radium-228 ($^{228}$Ra, half-life, 5.75 yr) is a naturally occurring radionuclide produced by the decay of $^{232}$Th, which is abundant in sediments and soils, and it is provided from rivers and sediments to seawater of the continental shelf (Moore, 1969; Nozaki et al., 1998). The activity concentration of $^{228}$Ra in surface seawater decreases as it is transported from the coast to the open ocean because of radioactive decay and eddy diffusion (Moore, 1972; Ku et al., 1995; Nozaki and Yamamoto, 2001). From a vertical profile of $^{228}$Ra, Moore (1972) estimated the rates of mixing across the thermocline, which brings nutrients from deeper layers to the euphotic zone. Coupled vertical profiles of $^{228}$Ra

and nutrients should provide an estimate of vertical flux of nutrients in the upper ocean. $^{228}$Ra has also been used as a tracer in studies on seawater mixing in coastal areas and above seafloors (Moore et al., 1986; Rutgers van der Loeff et al., 1995; Rutgers van der Loeff et al., 2003; Kadko and Muench, 2005; Nakano-Ohta and Sato, 2006; Kawakami and Kusakabe, 2008; Inoue et al., 2012; Inoue et al., 2016; Inoue et al., 2020), studies on the transport of particulate matter in the water column (Legeleux and Reyss, 1996; van Beek et al., 2007), and studies on the vertical flux of nutrients in the upper oceans (Ku et al., 1995; Nozaki and Yamamoto, 2001; Cai et al., 2002).

Ra-226 (half-life, 1600 yr) is also a naturally occurring radionuclide and it is produced from $^{230}$Th enriched in bottom sediments. The $^{226}$Ra activity concentration gradient from the coast to the ocean is lower than that of $^{228}$Ra due to the longer half-life of $^{226}$Ra. Recently, $^{226}$Ra and $^{228}$Ra along with the short-lived Ra isotopes $^{223}$Ra and $^{224}$Ra have been used for estimation of flux of submarine groundwater discharge (Kwon et al., 2014; Le Gland et al., 2017; Cho et al., 2018). Together with the distributions of nutrients and dissolved oxygen, these tracers have provided unique means to estimate the rates of metabolism in biogeochemical cycling.

The western subarctic Pacific Gyre (WSAG) is well known as a high nutrient, low chlorophyll area (HNLC), in which nutrients remain undepleted in surface waters throughout the year. In this area, phytoplankton growth is limited by iron (Fe) availability (Tsuda et al., 2003; Boyd et al., 2004), and the area has been reported to have the largest biological $CO_2$ drawdown among all the world's oceans (Takahashi et al., 2002). The high productivity of the region's ecosystem and fisheries (Sakurai, 2007) must be sustained by supplies of both Fe and nutrients entering the euphotic zone. The sub-surface pycnocline divides nutrient-poor surface mixed layers and nutrient-rich lower layers in the open ocean (Longhurst, 2007). The water exchange between these layers is regulated by the vertical eddy diffusivity that causes upward nutrient transport. Recent work (Nishioka et al., 2020) based on the combination of a comprehensive Fe observation dataset and vertical eddy diffusivity obtained by physical observations has implied that the formation of a high nutrient intermediate water pool, which is strongly influenced by lateral water transport from marginal seas (the Bering and Okhotsk Seas) and the existence of a nutrient return path from the intermediate water at potential density ($\sigma_\theta$) of 26.8-27.2 to the surface due to strong mixing around the Kuril and Aleutian Island chains are important for understanding how HNLC water is formed in the North Pacific. The horizontal distribution indicated by isopycnal analysis clearly presented evidence that the high, dissolved Fe source in the intermediate waters in the western subarctic Pacific is the marginal seas (Nishioka et al., 2020). Dissolved Fe concentration in the North Pacific Intermediate Water (NPIW) is high across a wide area in the western subarctic Pacific, particularly along the northern part of the WSAG including the areas southeast of the Kamchatka Peninsula, the western Bering Sea basin, and around the eastern Aleutian Islands. These findings suggest that clarifying the formation and pathways of NPIW is essential for a better

understanding of the mechanisms of biological production in the WSAG.

Around the WSAG, the shelf sediments in marginal seas, such as the East China Sea, Sea of Japan and Okhotsk Sea are known to play an important role in supplying Ra isotopes as well as nutrients (Kawakami and Kusakabe, 2008; Inoue et al., 2016). Then, Ra isotopes are supplied from the marginal seas, and they are laterally transported toward it. This signature and temporal change by radioactive decay can be used as a chronological tracer during advective transportation. The $^{226}$Ra and $^{228}$Ra activity concentrations in the Okhotsk Sea and around the Kuril Islands reported in the literature (Kawakami and Kusakabe, 2008; Inoue et al., 2016) were relatively high, indicating the possible influence of the continent and the continental shelf. However, $^{228}$Ra data were too limited to debate the contribution of lateral transportation from the margin. Especially, information on $^{228}$Ra activity concentrations in subsurface waters is not available in the WSAG, although such information could be key to resolving geochemical cycles for the lithogenic elements. In this study, we determined vertical profiles at Station K2 in the WSAG for concentrations of the natural radionuclides, $^{226}$Ra and $^{228}$Ra.

## EXPERIMENTAL

Seawater samples were collected using acid-cleaned 12 L NISKIN-X samplers with external springs mounted on a CTD-CMS at Station K2 (47°00'N, 165°00'E; **Figure 1A**) during a research cruise of the TS Oshoro-Maru from 19 May to 15 July 2016. Samples of 200 L were collected for $^{226}$Ra and $^{228}$Ra analyses at 10, 49, 99, 199, 397, and 594 m depths on 25-28 June.

The detailed procedures for $^{226}$Ra and $^{228}$Ra analyses can be found elsewhere (Nakano et al., 2008). In brief, a seawater sample was acidified by adding 1.8 L of 61% $HNO_3$. Then, 0.48 g of a minimally Ra-contaminated Ba carrier solution with Fe carrier (3 g of Fe) was added. After stirring for 15 min, 600 mL of 5% $Na_2SO_4$ solution was also added. 1.5 L of aqueous ammonium was gradually added to get a pH from 6 to 8. Ra isotopes were precipitated together with $BaSO_4$ and $Fe(OH)_3$ precipitates. The solution was allowed to stand for 24 h so that all particles sank to the bottom of the container. The precipitates were siphoned from the container and the supernatant was discarded by decantation. The yield of Ra isotopes was 82-96%, determined by gravimetric $BaSO_4$ yield.

Low-background gamma-spectrometry was performed on $BaSO_4$ fractions using Ge-detectors at the Ogoya Underground Laboratory, Japan (Hamajima and Komura, 2004). $^{226}$Ra ($^{214}$Pb; 295 and 352 keV) activity concentrations were calibrated using a mock-up sample prepared from a $BaSO_4$-$Fe(OH)_3$ mixture, a uranium standard issued from the New Brunswick Laboratory, USA (NBL-42-1) and KCl, while $^{228}$Ra ($^{228}$Ac; 338 and 911 keV) activity concentrations were based on a detection efficiency curve obtained from the mock-up sample. For each seawater sample, counting was typically performed over 3-7 d for $^{226}$Ra and $^{228}$Ra. Under the present analytical conditions, the lowest amounts of
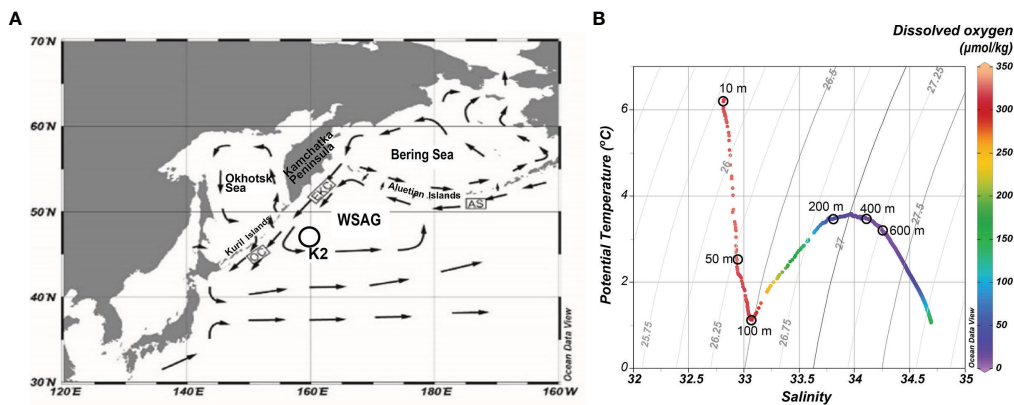
**FIGURE 1** | **(A)** Location of Station K2 in the western Subarctic Gyre (WSAG). The surface current system in the western North Pacific, the Bering Sea and the Okhotsk Sea is also displayed and it includes the East Kamchatka Current (EKC), Oyashio Current (OC), Alaskan Stream (AS). **(B)** Potential temperature-salinity diagram for K2 with oxygen concentration. Open circles shows sampling depths for Ra samples.

[228]Ra that can be determined in the seawater sample were ~4 mBq for 2-3 counting days, which yields a minimum detectable activity concentration of ~0.02 Bq m$^{-3}$ for [228]Ra using a 200 L seawater sample (Nakano et al., 2008). The concentrations of all radionuclides measured were decay-corrected based on the sampling date (Hamajima and Komura, 2004).

Nutrient (nitrate-plus-nitrite, phosphate, and silicate) concentrations were also analyzed in seawater samples collected from Station K2. Nutrient concentrations were measured using a BRAN-LUEBBE autoanalyzer (TRACCS 800) and a BL-Tec autoanalyzer (QuAAtro) (Gordon et al., 1992). Most of the nutrient measurements in this study were quality controlled using KANSO reference materials (KANSO Company).

Salinity and temperature were measured using a CTD sensor, and dissolved oxygen concentrations were measured using an oxygen sensor. The dissolved oxygen concentrations were also measured on board the ship by the Winkler titration method, and the dissolved oxygen concentrations obtained by the sensor (SBE 43 Dissolved Oxygen Sensor, Sea-Bird Scientific) were calibrated using those determined by the Winkler method (Carpenter, 1965). The eddy diffusivity $K_z$ value was measured using a free-fall vertical microstructure profiler (VMP500 Rockland Scientific International Co.).

## RESULTS AND DISCUSSION

### Hydrography

The elevated temperatures above the 50 m depth enhanced seasonal stratification in summer in the WSAG (**Figure 2A**). A subsurface temperature minimum (1.14°C) existed around the 100 m depth for which potential density was around 26.5 (**Figure 1B**); this was consistent with previous studies (e.g. Ueno and Yasuda, 2000). The mixed layer reaches more deeply in winter and it is overlaid by warmer and fresher water in summer (Yasuda, 1997). Low temperature water (<1.5°C) at

$\sigma_\theta$=26.5 was distributed along the East Kamchatka Current (EKC) from the western Bering Sea. Depths at $\sigma_\theta$=26.5 in the western Bering Sea and near the Bering Strait (around 50 - 70 m) were shallower than those in the WSAG. The vertical distribution of dissolved oxygen concentrations (**Figure 2D**) was almost constant from the surface to the depth of the temperature minimum. Macronutrients were at relatively high concentrations. The concentrations of silicate and nitrate were 1.4 μmol kg$^{-1}$, 18 μmol kg$^{-1}$, respectively, in surface water (**Figures 2E, F**). From these values, we thought it was likely that biological activity was controlled by another parameter, such as iron, in this HNLC area as has been reported in the literature (Nishioka et al., 2013; Nishioka et al., 2020).

The halocline increasing in salinity from 33.1 to 33.7 (**Figure 2B**) yielded the elevation of potential density, pycnocline ($\sigma_\theta$=26.5 – 26.8, **Figure 2C**) between 110 m and 160 m depth. In addition, this yielded a rapid increase of macronutrients by limitation of the vertical transportation. Potential temperature increased with depth and an intermediate maximum potential temperature of 3.57°C was observed at 250 m depth ($\sigma_\theta$=26.99), which generated a temperature inversion structure. The shallower temperature minimum layer and deeper temperature maximum layer called dichothermal and mesothermal waters, respectively, exist in the WSAG (Ueno and Yasuda, 2000; Ueno and Yasuda, 2005). All macronutrients rapidly increased with the decrease in dissolved oxygen concentration. Ueno and Yasuda (2000; 2005)also reported the dissolved oxygen concentration minimum was at 600 m. The present measurements showed the oxygen minimum layer (15.8-20.8 μmol kg$^{-1}$, $\sigma_\theta$=27.1-27.5 at 350–1000 m depth) was deeper than the temperature maximum.

Low-oxygen and high-silicate and high-nitrate water exist in the WSAG and Bering Gyre at the potential densities of 26.9 and 27.15, corresponding to 199 m and 397 m depths at Station K2, respectively (**Figure S1**). At shallower depths than $\sigma_\theta$=26.9, dissolved oxygen-rich water was observed along the EKC. Low dissolved oxygen water (<60 μmol/kg) at the potential density of
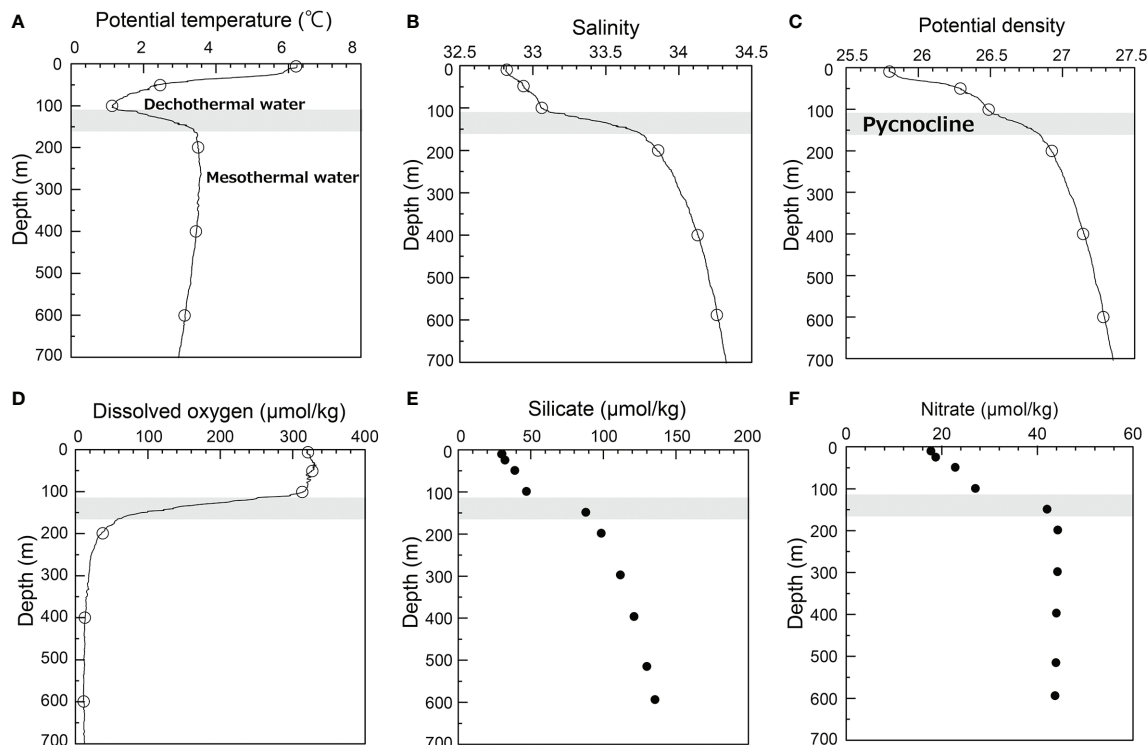
FIGURE 2 | Vertical profiles at Station K2 in the WSAG for: (A) potential temperature, (B) salinity and (C) potential density. Vertical profiles of concentrations at K2 for (D) dissolved oxygen and nutrients, (E) silicate and (F) nitrate. The gray band indicates the pycnocline overlying the mesothermal layer.

27.15, derived from the western Bering Sea, is found in the WSAG. Contrastingly, west of 155°E in the Oyashio Region and the Okhotsk Sea, high-dissolved oxygen water (>100 µmol/kg) is found. The Okhotsk Sea Intermediate Water (OSIW), characterized by relatively high-dissolved oxygen and dissolved Fe-rich water, flows out to the Pacific through the Kuril Straits, which has a strong influence on the extension region through the Oyashio Current. It propagates along the 26.8 $\sigma_\theta$ isopycnal surface to the western North Pacific (mainly west of 155°E). The hydrography at Station K2 we observed in this study indicated that the influence from the OSIW was minor. Station

K2 was located at the rim of the anti-clockwise gyre system (Figure 1A). The relatively lower salinity water signature (>33.8) at the potential density of 26.9 $\sigma_\theta$ can be traced back to the EKC along the Kamchatka Peninsula and the western Bering Gyre.

## Surface Ra Isotopes

Radium-226 activity concentrations were almost constant across the seasonal thermocline but slightly decreased with depth from the surface to 99 m, ranging from 1.9 to 2.2 Bq m$^{-3}$ (Table 1; Figure 3A), which corresponded to the depth above the pycnocline. Previous studies have reported surface distributions of

TABLE 1 | Activity concentrations of $^{226}$Ra and $^{228}$Ra and their ratios at station K2 in the western subarctic pacific gyre.

| Depth (m) | Potential Temperature (°C) | Potential density (kg m-3) | Salinity (psu) | Dissolved oxygen (µmol/kg) | Nitrate (µmol/kg) | Silicate (µmol/kg) | Phosphate (µmol/kg) | $^{226}$Ra(Bq m$^{-3}$) | $^{228}$Ra (Bq m$^{-3}$) | $^{228}$Ra/$^{226}$Ra |
|---|---|---|---|---|---|---|---|---|---|---|
| 10.2 | 6.092 | 25.821 | 32.824 | 328.8 | 17.7 | 29.9 | 1.47 | 2.24 ± 0.02 | 0.099 ± 0.017 | 0.044 ± 0.008 |
| 49.1 | 2.235 | 26.315 | 32.954 | 330.3 | 22.8 | 39.0 | 1.83 | 2.11 ± 0.03 | 0.099 ± 0.019 | 0.047 ± 0.009 |
| 99.3 | 1.390 | 26.483 | 33.117 | 295.5 | 27.1 | 47.0 | 2.10 | 1.94 ± 0.02 | 0.081 ± 0.017 | 0.042 ± 0.009 |
| 198.5 | 3.520 | 26.939 | 33.875 | 34.4 | 44.3 | 98.6 | 3.17 | 3.20 ± 0.04 | 0.067 ± 0.020 | 0.021 ± 0.006 |
| 396.5 | 3.437 | 27.161 | 34.141 | 17.8 | 44.0 | 121.2 | 3.18 | 3.20 ± 0.03 | 0.040 ± 0.011 | 0.012 ± 0.003 |
| 594.0 | 3.123 | 27.302 | 34.281 | 15.8 | 43.7 | 135.7 | 3.17 | 4.24 ± 0.03 | < 0.02 | < 0.005 |
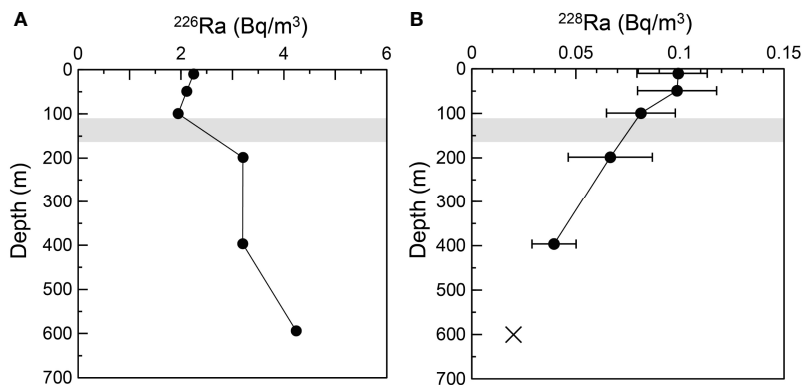
**FIGURE 3** | Vertical profiles at Station K2 in the WSAG for **(A)** $^{226}$Ra and **(B)** $^{228}$Ra activity concentrations. The letter x indicates the minimum detectable $^{228}$Ra activity concentration (0.02 Bq m$^{-3}$) in this study.

$^{226}$Ra activity concentrations in the western North Pacific involving the Kuroshio Extension area and the Okhotsk Sea (Nozaki et al., 1990; Kawakami and Kusakabe, 2008; Inoue et al., 2016; **Figure S1**), excluding the area in this study. Surface $^{226}$Ra activity concentration range was reported to be from 1.4 Bq m$^{-3}$ to 2.3 Bq m$^{-3}$ in the WSAG, and the present study was consistent with that. The presently obtained high $^{226}$Ra activity concentrations were comparable to those reported in the Bering Sea (1.3-2.5 Bq m$^{-3}$; Nozaki et al., 1990; Li et al., 2017; Inoue et al., 2020). Low $^{226}$Ra activity concentrations (0.6-1.2 Bq m$^{-3}$) have been observed in a coastal area along the Kamchatka Peninsula, which reflected freshwater input from the land (Inoue et al., 2016). On the other hand, $^{226}$Ra activity concentrations in the Kuroshio Current (1.0-1.4 Bq m$^{-3}$) and Kuroshio Extension (1.1-1.5 Bq m$^{-3}$) areas (Yamada and Nozaki, 1986; Nozaki et al., 1990; Kawakami and Kusakabe, 2008) were found to be lower than those of the subarctic region. $^{226}$Ra activity concentrations in the Alaskan Gyre (1.4-1.9 Bq m$^{-3}$, Nozaki et al., 1990) were also lower than those of the WSAG and the Bering Sea.

The $^{226}$Ra distribution trend resembled those of silicate and nitrate, which indicated $^{226}$Ra was supplied from subsurface water by vertical transport processes. A high $^{226}$Ra activity concentration (2.3 Bq m$^{-3}$) in the surface was also observed in the Okhotsk Sea and Oyashio Current area (Inoue et al., 2016). Broecker et al. (1976) and Nozaki et al. (1990) showed $^{226}$Ra in surface waters linearly correlated with dissolved silicate. Both these groups also reported that like silicate, surface $^{226}$Ra was derived from the deeper layer. Nozaki et al. (1990) noted that $^{226}$Ra in surface waters linearly correlated with dissolved silicate concentration with a best fit line of [$^{226}$Ra (Bq m$^{-3}$)] = 1.3 + 0.021 [SiO$_2$ (μmol kg$^{-1}$)] for the North Pacific. Our $^{226}$Ra activity concentration at 10 m agreed with the calculated $^{226}$Ra activity concentration based on the silicate concentration. In addition, deeper water to 600 m also followed this best fit relationship, which indicated that both $^{226}$Ra and silicate were supplied from subsurface and deeper water in the WSAG. The dataset of $^{226}$Ra and silicate concentrations in the Okhotsk Sea is limited in the Kuril

Basin (Inoue et al., 2016), but there is a difference between $^{226}$Ra and silicate concentrations in the Okhotsk Sea as can be seen in **Figure S2**. High $^{226}$Ra activity concentration in the Kuril basin in the Okhotsk Sea was reported with lower concentrations of macronutrients than those in the WSAG, which reflected $^{226}$Ra released from the shelf sediments in the Okhotsk Sea (Kawakami and Kusakabe, 2008).

We found $^{228}$Ra activity concentrations in the mixed layer were 0.099 ± 0.017 Bq m$^{-3}$ at 10 m depth and 0.099 ± 0.019 Bq m$^{-3}$ at 49 m depth (**Figure 3B**). $^{228}$Ra activity concentration (0.081 ± 0.017) at 99 m above the pycnocline was slightly lower than that of the upper layer. Nozaki et al. (1990) suggested that the effect of radioactive decay of $^{228}$Ra in the surface layer was much smaller than the effect of lateral transportation and mixing due to the rapid surface velocity. The surface distribution in the North Pacific seemingly reflected spatial variabilities of the $^{228}$Ra source (**Figure S1**). Low $^{228}$Ra activity concentrations were reported in the WSAG (0.1 Bq m$^{-3}$; this study and Inoue et al., 2016) and the Bering Sea Gyre (0.04 - 0.09 Bq m$^{-3}$; Nozaki et al., 1990; Li et al., 2017; Inoue et al., 2020). Hydrographic data (**Figure 1**) indicated that the Okhotsk Sea water did not influence our observation at Station K2 in the WSAG and EKC dominated the surface layer. There are high $^{228}$Ra source regions in the Okhotsk Sea (0.49 – 0.98 Bq m$^{-3}$; Kawakami and Kusakabe, 2008; Inoue et al., 2016), Sea of Japan (1.5-2.2 Bq m$^{-3}$; Inoue et al., 2012) and shelf and shelf slope in the Bering Sea (0.3-0.9 Bq m$^{-3}$, Li et al., 2017; Inoue et al., 2020). $^{228}$Ra is supplied from sediments in the continental shelf, which differs from $^{226}$Ra supplied from sub-surface and deep water in the WSAG. Contrary to $^{226}$Ra, $^{228}$Ra, a short half-life radionuclide, is depleted in the deeper layers by radioactive decay. $^{228}$Ra activity concentration in the Sea of Japan is higher than those in the Kuril Basin in the Okhotsk Sea. Surface water from the Sea of Japan passes through the Tsugaru Strait and has an impact on surface $^{228}$Ra in the Kuroshio-Oyashio Transition Zone (0.25 to 1.51 Bq m$^{-3}$). Therefore, the relative contribution of $^{228}$Ra from the margins is larger than that of $^{226}$Ra in the WSAG.

## Vertical Profiles of Ra Isotopes

The dataset of $^{226}$Ra and $^{228}$Ra vertical profiles we obtained in this study is the first reported for the WSAG. $^{226}$Ra activity concentrations in the dichothermal water at 100 m below the seasonal thermocline were consistent with those in surface water (**Figure 3A**). Below the pycnocline, $^{226}$Ra activity concentrations between 110 and 160 m increased with depth. $^{226}$Ra activity concentrations were constant (3.2 Bq m$^{-3}$) at 199 m and 397 m depths, then increased to 4.2 Bq m$^{-3}$ at 594 m. We observed that $^{226}$Ra in deeper waters from 199 m to 594 m also followed the linear relationship with silicate concentrations as seen in the surface layer. This feature was consistent with our understanding that $^{226}$Ra was vertically supplied from a deeper layer in a high latitude area, such as the WSAG.

Radium-228 activity concentrations gradually decreased with depth from 0.08 Bq m$^{-3}$ at 10 m to 0.04 ± 0.01 Bq m$^{-3}$ at 399 m. $^{228}$Ra activity concentrations was less than the detectable level (<0.02 Bq m$^{-3}$) at 594 m depth. The vertical distribution of $^{228}$Ra activity concentrations was in contrast to that of $^{226}$Ra activity concentrations due to radioactive decay in the deeper layer. In addition, $^{228}$Ra activity concentrations below the pycnocline were much lower compared with $^{228}$Ra activity concentrations obtained in marginal seas such as the southwest Okhotsk Sea (0.3-0.4 Bq m$^{-3}$; Inoue et al., 2012) and the Sea of Japan (0.1-0.2 Bq m$^{-3}$; Okubo, 1980). We concluded that both Ra isotopes and their activity ratios are good tracers to identify the source of intermediate water in the WSAG. We also note that detectable $^{228}$Ra exists below the pycnocline, nevertheless vertical stratification is obvious in the WSAG due to low salinity in the mixed layer. Since $^{228}$Ra decreases by radioactive decay with a half-life of 5.8 yr, the $^{228}$Ra activity concentration and $^{228}$Ra/$^{226}$Ra activity ratio can be used as a transient tracer for horizontal transport when underlying waters are isolated from the surface layer and a new supply is lacking.

Our $^{228}$Ra measurements were limited to water layers above 600 m and sparse due to the need for time-consuming large-volume water sampling during a short cruise. However, ultra-low background gamma-ray detection is possible for a low minimum detectable activity. To calculate the inventory of $^{228}$Ra in the water column, we interpolated $^{228}$Ra activity concentrations with depth between the surface to 397 m. $^{228}$Ra activity concentrations below 397 m depth were extrapolated using the relationship from 199 to 397 m depths. $^{228}$Ra activity concentrations were assumed

to decrease with depth and reach zero around 700 m depth. Calculated $^{228}$Ra activity concentration at 600 m depth was 0.01 Bq m$^{-3}$, which was lower than the detectable $^{228}$Ra activity concentration (0.02 Bq m$^{-3}$).

## Vertical Flux Estimation of $^{228}$Ra

We examined the inventory of $^{228}$Ra between depth $z_1$ and $z_2$ in the water column as:

$$^{228}Ra_{inventory,\ z1-Z2} = \int_{z1}^{Z2} {}^{228}Ra(z)dz. \tag{1}$$

Calculated $^{228}$Ra inventories are shown in **Table 2**. $^{228}$Ra inventories below the depth $z_1$ to bottom are also shown. $^{228}$Ra inventories in the mixed layer (0 to 50 m) and dichothermal layer (50 to 110 m) was 5.0 Bq m$^{-2}$ and 5.3 Bq m$^{-1}$, respectively. On the other hand, $^{228}$Ra inventories in the mesothermal layer underlying the pycnocline (below 160 m depth) was 19.4 Bq m$^{-2}$, which was comparable to the inventory in the surface layer.

Here, if we assumed the steady state, supply of $^{228}$Ra ($F_{Ra-228}$) should be balanced with the reduction rate of $^{228}$Ra inventory by radioactive decay as the following equation.

$$R_{Ra-228} = \lambda_{228\,Ra} \times {}^{228}Ra_{inventory,\ below\ z} \tag{2}$$

Here, $\lambda^{228}Ra$ is decay constant of $^{228}$Ra (3.82 × 10$^{-9}$ s$^{-1}$). Ku et al. (1995) and Nozaki and Yamamoto (2001) reported that $^{228}$Ra in the mixed layer was transported downwardly by vertical eddy diffusion (one-dimensional model) and its inventory was decreased by radioactive decay. We did not consider other possible processes, such as lateral advection, biological uptake and regeneration processes, in accordance with previous studies (Ku et al., 1995; Nozaki and Yamamoto, 2001).

In addition, $^{228}$Ra below the pycnocline could be supplied only from the upper water by vertical eddy diffusion. We calculated the vertical eddy diffusive flux of $^{228}$Ra ($F_{Ra-228}$) across the depth horizon $z$ as the product of vertical eddy diffusivity $K_z$ (m$^2$ s$^{-1}$) obtained from turbulence observation using microstructure profiler and vertical gradient of $^{228}$Ra activity concentration, ($\partial\,^{228}Ra / \partial z$) in the depth profile (**Table 3**).

$$F_{Ra-228} = -K_z \times \left( \frac{\partial\,^{228}Ra}{\partial z} \right)_z \tag{3}$$

**TABLE 2 |** $^{228}$Ra inventory reduction rate by radioactive decay.

| | Depth (m) | | $^{228}$Ra activity concentration (Bq m$^{-3}$) | $^{228}$Ra inventory $z_1$-$z_2$ (Bq m$^{-2}$) | $^{228}$Ra inventory below $z_1$ (Bq m$^{-3}$) | Reduction rate of $^{228}$Ra by radioactive decay $R_{Ra-228}$ (Bq m$^{-2}$ d$^{-1}$) |
|---|---|---|---|---|---|---|
| | $z_1$ | $z_2$ | | | | |
| Mixed layer | 0 - | 50 | 0.099 | 5.0 | 33.4 | 0.0110 |
| Dichothermal layer | 50 - | 110 | 0.099 | 5.3 | 28.5 | 0.0094 |
| Pycnocline | 110 - | 160 | 0.078 | 3.7 | 23.2 | 0.0076 |
| Mesothermal layer | 160 - | | 0.072 | 19.4 | 19.4 | 0.0064 |

Comparison between [228]Ra diffusive flux and reduction rate by radioactive decay.

| Depth(m) | $K_z$(m$^2$ s$^{-1}$) | dRa/dz(Bq m$^{-4}$) | [228]Ra diffusive flux $F_{Ra-228}$(Bq m$^{-2}$ d$^{-1}$) | $F_{Ra-228}/R_{Ra-228}$ |
|---|---|---|---|---|
| 10 | 0.0159 | – | – | – |
| 25 | 0.0080 | – | – | – |
| 50 | 0.0000096 | -0.000017 | 0.000014 | 0.1% |
| 100 | 0.0000019 | -0.00014 | 0.000024 | 0.3% |
| 125 | 0.0000023 | -0.00015 | 0.000029 | 0.4% |
| 150 | 0.0000027 | -0.00015 | 0.000034 | 0.4% |
| 175 | 0.0000038 | -0.00015 | 0.000048 | 0.8% |
| 200 | 0.0000049 | -0.00014 | 0.000060 | 0.9% |
| 225 | 0.0000053 | -0.00014 | 0.000062 | 1.0% |
| 250 | 0.0000056 | -0.00014 | 0.000066 | 1.0% |

The [228]Ra activity concentrations were uniform in the mixed layer (0-50 m) and no vertical concentration gradient could be distinguished. On the other hand, the vertical eddy diffusive flux of [228]Ra entraining in the deeper layer and crossing over the pycnocline was ranged from 0.000029 Bq m$^{-2}$ d$^{-1}$ (125 m) to 0.000034 Bq m$^{-2}$ d$^{-1}$ (150 m). It was two orders of magnitude smaller (0.4%) than the reduction rate of [228]Ra inventory in the water column even if a large uncertainty of vertical gradients of [228]Ra activity concentration derived from [228]Ra analysis was considered. Assuming the steady state, the imbalance between the fluxes strongly suggested that [228]Ra below the mixed layer was supplied by lateral advection.

According to Ku et al. (1995), nitrate flux between 100 m and 200 m was estimated as 3-10 mmol m$^{-2}$ d$^{-1}$ by using vertical profiles of [228]Ra and nitrate, and the [228]Ra-based diffusive nitrate flux in this study was in the same range. Previously, Nozaki and Yamamoto (2001) also calculated nitrate fluxes in the eastern Indian Ocean, and pointed out the lateral transport of [228]Ra might elevate activity concentrations of [228]Ra in intermediate water, resulting in overestimation of the fluxes. Here, we considered this was the case in the WSAG. The nitrate flux range based on the [228]Ra profile was two to four orders of magnitude greater than the reported values in the subarctic

Pacific (0.03-0.7 mmol m$^{-2}$ d$^{-1}$; Nishioka et al., 2020). This discrepancy implied [228]Ra below the pycnocline in the WSAG was supplied from lateral advection. Nishioka et al. (2020) reported that the nitrate fluxes were largest in the Kuril Straits (~100 mmol m$^{-2}$ d$^{-1}$) and second largest along the Aleutian Islands (~10 mmol m$^{-2}$ d$^{-1}$), which was caused only by enhanced turbulent diapycnal mixing near the marginal area (Itoh et al., 2010; Itoh et al., 2011; Yagi and Yasuda, 2012). It is important to study the [228]Ra source and its supply process to mesothermal water in the intermediate depth for better understanding of biogeochemical cycles of nutrients in the WSAG. Low-oxygen and high-silicate and high-nitrate water are found in the WSAG and Bering Gyre at the isopycnal surfaces of 26.9 and 27.15, corresponding to 199 m and 397 m depths at Station K2, respectively (**Figure S2**). We could trace the relatively lower salinity water signature (>33.8) at $\sigma_\theta$ = 26.9 back to the EKC along the Kamchatka Peninsula and the western Bering Gyre.

Higher [228]Ra/[226]Ra ratios were reported near the Kamchatka Peninsula in the WSAG and in the Bering Gyre. The highest ratio (0.15) was reported for the continental shelf area in the Bering Sea (Li et al., 2017; Inoue et al., 2020). Assuming simple mixing between surface water in the continental shelf in the Bering Sea ([228]Ra/[226]Ra =0.15, salinity = 32.8; Inoue et al., 2020) and



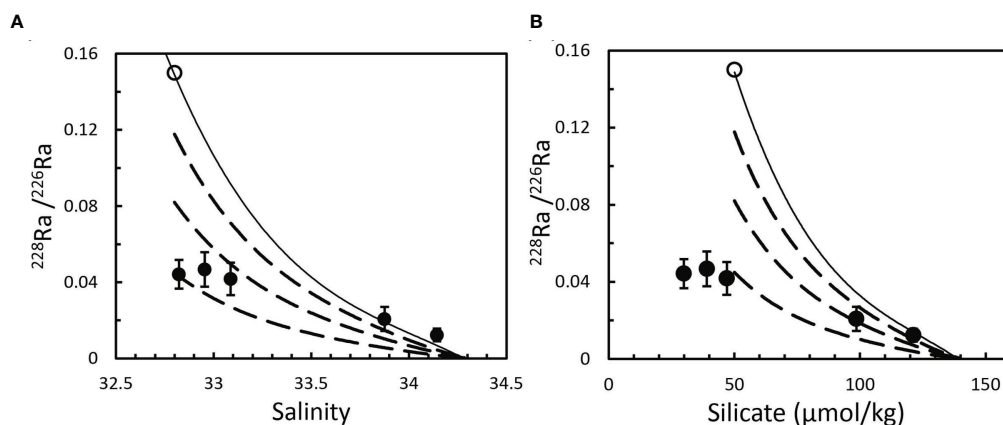**FIGURE 4 |** Relationships of [228]Ra/[226]Ra activity ratio with **(A)** salinity and **(B)** silicate concentration. Open circles indicate previously observed data in the continental shelf in the Bering Sea (Inoue et al., 2020). The solid lines are the mixing curves between the oxygen minimum layer and surface water in the continental shelf in the Bering Sea. The dashed lines are considered to represent [228]Ra depletion by radioactive decay at elapsed times of 2, 5, and 10 yr before mixing.

intermediate water at the oxygen minimum layer ($^{228}$Ra/$^{226}$Ra =0, salinity = 34.3) without radioactive decay, the calculated $^{228}$Ra/$^{226}$Ra in the mesothermal layer exceeded the observed values (**Figure 4**). If the surface water in the continental shelf was penetrated within 2 years for salinity and 7 years for silicate, the calculated ratios were close to the observed values. To investigate the lateral transport process of Ra isotopes in the WSAG, we need more information on the possible $^{228}$Ra sources near the Kamchatka Peninsula and the Bering Gyre.

## CONCLUSION

The vertical distributions of the Ra isotopes, $^{226}$Ra and $^{228}$Ra, were determined for the first time from large-volume seawater sampling done at Station K2 in the western Subarctic Pacific Gyre (WSAG).

1. The $^{228}$Ra activity concentrations in the surface layer were controlled by the mixture of the low-$^{228}$Ra activity concentration EKC water and the high-$^{228}$Ra activity concentration surface water in the Okhotsk Sea, and the $^{228}$Ra activity concentrations were highly correlated with salinity in the WSAG.
2. The vertical distributions of $^{226}$Ra and $^{228}$Ra activity concentrations were uniform from the surface to the dichothermal layer of 100 m depth due to vertical mixing in winter.
3. $^{228}$Ra activity concentrations decreased with water depth below the main pycnocline. The vertical transport by eddy diffusion was concluded to be a minor process for the $^{228}$Ra flux, and the horizontal transport possibly supplied $^{228}$Ra in the intermediate mesothermal water (200-400 m depths) in the open ocean in the WSAG.
4. Observed $^{228}$Ra activity concentrations in the mesothermal layer implied that water with a relatively high $^{228}$Ra/$^{226}$Ra activity ratio, which can be found in the EKC, was supplied to the interior of the WSAG and laterally advected.

## DATA AVAILABILITY STATEMENT

The original contributions presented in the study are included in the article/**Supplementary Material**. Further inquiries can be directed to the corresponding author.

## AUTHOR CONTRIBUTIONS

HT and HO wrote the first draft of the manuscript. TH, JN, and MI performed the experiments and statistical analysis. HT, HO, and TT contributed to the conception and design of the study. All authors contributed to manuscript revision, read, and approved the submitted version.

## FUNDING

## ACKNOWLEDGMENTS

## SUPPLEMENTARY MATERIAL

The Supplementary Material for this article can be found online at: https://www.frontiersin.org/articles/10.3389/fmars.2022.824862/full#supplementary-material

## REFERENCES

Boyd, P. W., Law, C. S., Wong, C. S., Nojiri, Y., Tsuda, A., Levasseur, M., et al. (2004). The Decline and Fate of an Iron-Induced Subarctic Phytoplankton Bloom. *Nature* 428 (6982), 549–553. doi: 10.1038/nature02437

Broecker, W. S., Doddard, J., and Sarmiento, J. (1976). The Distribution of $^{226}$Ra in the Atlantic Ocean. *Ear. Planet. Sci. Lett.* 32, 220–235. doi: 10.1016/0012-821X(76)90063-7

Cai, P., Huang, Y., Chen, M., Guo, L., Li, G., and Qiu, Y. (2002). New Production Based on $^{228}$Ra-Derived Nutrient Budgets and Thorium-Estimated POC Export at the Intercalibration Station in the South China Sea. *Deep-Sea. Res. Pt. I.* 49 (1), 53–66. doi: 10.1016/S0967-0637(01)00040-1

Carpenter, J. H. (1965). The Chesapeake Bay Institute Technique for the Winkler Dissolved Oxygen Method. *Limnol. Oceanogr.* 10, 141–143. doi: 10.4319/lo.1965.10.1.0141

Cho, H. M., Kim, G., Kwon, E. Y., Moosdorf, N., Garcia-Orellana, J., and Santos, I. R. (2018). Radium Tracing Nutrient Inputs Through Submarine Groundwater Discharge in the Global Ocean. *Sci. Rep.* 8 (1), 2439. doi: 10.1038/s41598-018-20806-2

Gordon, L. I., Jennings, J. C.Jr., Ross, A. A., and Krest, J. M. (1992). An Suggested Protocol for Continuous Flow Automated Analysis of Seawater Nutrients (Phosphate, Nitrate, Nitrite and Silicic Acid) in the WOCE Hydrographic Program and the Joint Global Ocean Fluxes Study, OSU Coll. Of Oc. *Descr. Chem. Oc. Grp. Tech. Rpt.* 92-1

Hamajima, Y., and Komura, K. (2004). Background Components of Ge Detectors in Ogoya Underground Laboratory. *Appl. Radiat. Isot.* 61, 179–183. doi: 10.1016/j.apradiso.2004.03.041

Inoue, M., Shirotani, Y., Nagao, S., Kofuji, H., Volkov, Y. N., and Nishioka, J. (2016). Migration of the FDNPP-Derived $^{134}$Cs and $^{137}$Cs Along With $^{226}$Ra and $^{228}$Ra Concentrations Across the Northwestern North Pacific Ocean. *J. Environ. Radioact.* 162–163, 33–38. doi: 10.1016/j.jenvrad.2016.05.011

Inoue, M., Takehara, R., Hanaki, S., Kameyama, H., Nishioka, J., and Nagao, S. (2020). Distributions of Radiocesium and Radium Isotopes in the Western Bering Sea in 2018. *Mar. Chem.* 225, 103843. doi: 10.1016/j.marchem.2020.103843

Inoue, M., Yoshida, K., Minakawa, M., Kofuji, H., Nagao, S., Hamajima, Y., et al. (2012). Spatial Variations of $^{226}$Ra, $^{228}$Ra, $^{137}$Cs and $^{228}$Th Activities in the Southwestern Okhotsk Sea. *J. Environ. Radioact.* 104, 75–80. doi: 10.1016/j.jenvrad.2011.09.007

Itoh, S., Yasuda, I., Nakatsuka, T., Nishioka, J., and Volkov, Y. N. (2010). Fine- and Microstructure Observations in the Urup Strait, Kuril Islands, During August 2006. *J. Geophys. Res.: Ocean.* 115 (C08004), 1–12. doi: 10.1029/2009JC005629

Itoh, S., Yasuda, I., Yagi, M., Osafune, S., Kaneko, H., Nishioka, J., et al. (2011). Strong Vertical Mixing in the Urup Strait, *Geophys. Res. Lett.* 38 (16). doi: 10.1029/2011GL048507

Kadko, D., and Muench, R. (2005). Evaluation of Shelf–Basin Interaction in the Western Arctic by Use of Short-Lived Radium Isotopes: The Importance of Mesoscale Processes. *Deep-Sea. Res. Pt. II.* 52 (24), 3227–3244. doi: 10.1016/j.dsr2.2005.10.008

Kawakami, H., and Kusakabe, M. (2008). Surface Water Mixing Estimated From $^{228}$Ra and $^{226}$Ra in the Northwestern North Pacific. *J. Environ. Radioact.* 99 (8), 1335–1340. doi: 10.1016/j.jenvrad.2008.04.011

Ku, T. L., Luo, S., Kusakabe, M., and Bishop, J. K. B. (1995). $^{228}$Ra-Derived Nutrient Budgets in the Upper Equatorial Pacific and the Role of "New" Silicate in Limiting Productivity. *Deep. Sea. Res. Pt. II.* 42 (2), 479–497. doi: 10.1016/0967-0645(95)00020-Q

Kwon, E. Y., Kim, G., Primeau, F., Moore, W. S., Cho, H. M., De Vries, T., et al. (2014). Global Estimate of Submarine Groundwater Discharge Based on an Observationally Constrained Radium Isotope Model. *Geophys. Res. Lett.* 41 (23), 8438–8444. doi: 10.1002/2014gl061574

Legeleux, F., and Reyss, J. L. (1996). $^{228}$Ra/$^{226}$Ra Activity Ratio in Oceanic Settling Particles: Implications Regarding the Use of Barium as a Proxy for Paleoproductivity Reconstruction. *Deep. Sea. Res. Pt. I.: Ocean.* 43 (11), 1857–1863. doi: 10.1016/S0967-0637(96)00086-6

Le Gland, G., Mémery, L., Aumont, O., and Resplandy, L. (2017). Improving the Inverse Modeling of a Trace Isotope: How Precisely can Radium-228 Fluxes Toward the Ocean and Submarine Groundwater Discharge be Estimated? *Biogeosciences* 14 (13), 3171–3189. doi: 10.5194/bg-14-3171-2017

Li, Q., Chen, M., Jia, R., Zeng, J., Lin, H., Zhen, M., et al. (2017). Transit Time of River Water in the Bering and Chukchi Seas Estimated From $\delta^{18}$O and Radium Isotopes. *Prog. Oceanogr.* 159, 115–129. doi: 10.1016/j.pocean.2017.08.004

Longhurst, A. (2007). *Ecological Geography of the Sea* (London: Academic Press). doi: 10.1016/B978-012455521-1/50002-4

Moore, W. S. (1969). Measurement of Ra228 and Th228 in Sea Water. *J. Geophys. Res.* 74 (2), 694–704. doi: 10.1029/JB074i002p00694

Moore, W. S. (1972). Radium-228: Application to Thermocline Mixing Studies. *Earth. Planet. Sci. Lett.* 16 (3), 421–422. doi: 10.1016/0012-821X(72)90161-6

Moore, W. S., Sarmiento, J. L., and Key, R. (1986). Tracing the Amazon Component of Surface Atlantic Water Using $^{228}$Ra, Salinity and Silica. *J. Geophys. Res.: Ocean.* 91 (C2), 2574–2580. doi: 10.1029/JC091iC02p02574

Nakano, Y., Inoue, M., and Komura, K. (2008). Simple Coprecipitation Method Combined With Low-Background γ-Spectrometry: Determination of $^{7}$Be, $^{137}$Cs, $^{210}$Pb, and Radium and Thorium Isotopes in Small-Volume Coastal Water Samples. *J. Oceanogr.* 64 (5), 713–717. doi: 10.1007/s10872-008-0060-y

Nakano-Ohta, T., and Sato, J. (2006). Determination of $^{228}$Ra and $^{226}$Ra in Seawater Collected on Manganese-Impregnated Acrylic Fiber. *Radioisotopes* 55 (8), 443–449. doi: 10.3769/radioisotopes.55.443

Nishioka, J., Nakatsuka, T., Watanabe, Y. W., Yasuda, I., Kuma, K., Ogawa, H., et al. (2013). Intensive Mixing Along an Island Chain Controls Oceanic Biogeochemical Cycles. *Global Biogeochem. Cy.* 27 (3), 920–929. doi: 10.1002/gbc.20088

Nishioka, J., Obata, H., Ogawa, H., Ono, K., Yamashita, Y., Lee, K., et al. (2020). Subpolar Marginal Seas Fuel the North Pacific Through the Intermediate Water at the Termination of the Global Ocean Circulation. *Proc. Natl. Acad. Sci. U.S.A.* 117 (23), 12665–12673. doi: 10.1073/pnas.2000658117

Nozaki, Y., Dobashi, F., Kato, Y., and Yamamoto, Y. (1998). Distribution of Ra Isotopes and the 210Pb and 210Po Balance in Surface Seawaters of the Mid Northern Hemisphere. *Deep. Sea. Res. Pt. I.: Ocean.* 45 (8), 1263–1284. doi: 10.1016/S0967-0637(98)00016-8

Nozaki, Y., Kasemsupaya, V., and Tsubota, H. (1990). The Distribution of $^{228}$Ra and $^{226}$Ra in the Surface Waters of the Northern North Pacific. *Geochem. J.* 24 (1), 1–6. doi: 10.2343/geochemj.24.1

Nozaki, Y., and Yamamoto, Y. (2001). Radium 228 Based Nitrate Fluxes in the Eastern Indian Ocean and the South China Sea and a Silicon-Induced "Alkalinity Pump" Hypothesis. *Global Biogeochem. Cy.* 15 (3), 555–567. doi: 10.1029/2000gb001309

Okubo, T. (1980). Radium-228 in the Japan Sea. *J. Oceanogr. Soc Japan.* 36 (5), 263–268. doi: 10.1007/BF02072128

Rutgers van der Loeff, M. M., Key, R. M., Scholten, J., Bauch, D., and Michel, A. (1995). $^{228}$Ra as a Tracer for Shelf Water in the Arctic Ocean. *Deep-Sea. Res. Pt. II.* 42 (6), 1533–1553. doi: 10.1016/0967-0645(95)00053-4

Rutgers van der Loeff, M. M., Kühne, S., Wahsner, M., Höltzen, H., Frank, M., Ekwurzel, B., et al. (2003). $^{228}$Ra and $^{226}$Ra in the Kara and Laptev Seas. *Cont. Shelf Res.* 23 (1), 113–124. doi: 10.1016/S0278-4343(02)00169-3

Sakurai, Y. (2007). An Overview of the Oyashio Ecosystem. *Deep-Sea. Res. Pt. II.* 54 (23), 2526–2542. doi: 10.1016/j.dsr2.2007.02.007

Takahashi, T., Sutherland, S. C., Sweeney, C., Poisson, A., Metzl, N., Tilbrook, B., et al. (2002). Global Sea–Air $CO_2$ Flux Based on Climatological Surface Ocean $P$co$_2$, and Seasonal Biological and Temperature Effects. *Deep-Sea. Res. Pt. II.* 49 (9), 1601–1622. doi: 10.1016/S0967-0645(02)00003-6

Tsuda, A., Takeda, S., Saito, H., Nishioka, J., Nojiri, Y., Kudo, I., et al. (2003). A Mesoscale Iron Enrichment in the Western Subarctic Pacific Induces a Large Centric Diatom Bloom. *Science* 300 (5621), 958–961. doi: 10.1126/science.1082000

Ueno, H., and Yasuda, I. (2000). Distribution and Formation of the Mesothermal Structure (Temperature Inversions) in the North Pacific Subarctic Region. *J. Geophys. Res.: Ocean.* 105 (C7), 16885–16897. doi: 10.1029/2000JC900020

Ueno, H., and Yasuda, I. (2005). Temperature Inversions in the Subarctic North Pacific. *J. Phys. Oceanogr.* 35 (12), 2444–2456. doi: 10.1175/jpo2829.1

van Beek, P., François, R., Conte, M., Reyss, J. L., Souhaut, M., and Charette, M. (2007). $^{228}$Ra/$^{226}$Ra and $^{226}$Ra/Ba Ratios to Track Barite Formation and Transport in the Water Column. *Geochim. Cosmochim. Acta* 71 (1), 71–86. doi: 10.1016/j.gca.2006.07.041

Yagi, M., and Yasuda, I. (2012). Deep Intense Vertical Mixing in the Bussol' Strait. *Geophys Res. Lett.* 39 (1), 1–5. doi: doi:10.1029/2011GL050349

Yamada, M., and Nozaki, Y. (1986). Radium Isotopes in Coastal and Open Ocean Surface Waters of the Western North Pacific. *Mar. Chem.* 19 (4), 379–389. doi: 10.1016/0304-4203(86)90057-5

Yasuda, I. (1997). The Origin of the North Pacific Intermediate Water. *J. Geophys. Res.: Ocean.* 102 (C1), 893–909. doi: 10.1029/96JC02938